Quantum dimer model for the pseudogap metal

Matthias Punk[a,b,c], Andrea Allais[d], and Subir Sachdev[d,e,1]

[a]Institute for Theoretical Physics, University of Innsbruck, 6020 Innsbruck, Austria; [b]Institute for Quantum Optics and Quantum Information, Austrian Academy of Sciences, 6020 Innsbruck, Austria; [c]Physics Department, Ludwig-Maximilians-Universität München, 80333 Munich, Germany; [d]Department of Physics, Harvard University, Cambridge, MA 02138; and [e]Perimeter Institute for Theoretical Physics, Waterloo, Ontario N2L 2Y5, Canada

We propose a quantum dimer model for the metallic state of the hole-doped cuprates at low hole density, p. The Hilbert space is spanned by spinless, neutral, bosonic dimers and spin $S = 1/2$, charge $+e$ fermionic dimers. The model realizes a "fractionalized Fermi liquid" with no symmetry breaking and small hole pocket Fermi surfaces enclosing a total area determined by p. Exact diagonalization, on lattices of sizes up to 8×8, shows anisotropic quasiparticle residue around the pocket Fermi surfaces. We discuss the relationship to experiments.

spin liquid | Fermi liquid | dimer model | superconductivity

The recent experimental progress in determining the phase diagram of the hole-doped Cu-based high-temperature superconductors has highlighted the unusual and remarkable properties of the pseudogap (PG) metal (Fig. 1). A characterizing feature of this phase is a depletion of the electronic density of states at the Fermi energy (1, 2), anisotropically distributed in momentum space, that persists up to room temperature.

Attempts have been made to explain the pseudogap metal using thermally fluctuating order parameters; we argue below that such approaches are difficult to reconcile with recent transport experiments. Instead, we introduce a new microscopic model that realizes an alternative perspective (3), in which the pseudogap metal is a finite temperature (T) realization of an interesting quantum state: the fractionalized Fermi liquid (FL*). We show that our model is consistent with key features of the pseudogap metal observed by both transport and spectroscopic probes.

The crucial observation that motivates our work is the tension between photoemission and transport experiments. In the cuprates, the hole density p is conventionally measured relative to that of the insulating antiferromagnet (AF), which has one electron per site in the Cu d band. Therefore, the hole density relative to a filled Cu band, with two electrons per site, is actually $1 + p$. In fact, photoemission experiments at large hole doping observe a Fermi surface enclosing an area determined by the hole density $1 + p$ (4), in agreement with the Luttinger relation. In contrast, in the pseudogap metal, a mysterious "Fermi arc" spectrum is observed (5–7), with no clear evidence of closed Fermi surfaces. However, despite this unusual spectroscopic feature, transport measurements report vanilla Fermi liquid properties, but associated with carrier density p, rather than $1 + p$. The carrier density of p was indicated directly in Hall measurements (8), whereas other early experiments indicated suppression of the Drude weight (9–11). Although the latter could be compatible with a carrier density of $1 + p$ but with a suppressed kinetic term, the Hall measurements indicate the suppression of the Drude weight is more likely due to a small carrier density. Two recent experiments displaying Fermi liquid behavior at low p are especially notable: (*i*) the quasiparticle lifetime $\tau(\omega, T)$ determined from optical conductivity experiments (12) has the Fermi liquid-like dependence $1/\tau \propto (\hbar\omega)^2 + (c\pi k_B T)^2$, with c an order unity constant; and (*ii*) the in-plane magnetoresistance of the pseudogap (13) is proportional to $\tau^{-1}(1 + bH^2\tau^2 + \dots)$ in an applied field H, where $\tau \sim T^{-2}$ and b is a T-independent constant; this is Kohler's rule for a Fermi liquid.

It is difficult to account for the nearly perfect Fermi liquid-like T dependence in transport properties of the pseudogap in a

theory in which a large Fermi surface of size $1 + p$ (14) is disrupted by a thermally fluctuating order. In such a theory, we expect that transport should instead reflect the T dependence of the correlation length of the order.

Moreover, a reasonable candidate for the fluctuating order has not yet been identified. The density wave (DW) order present at lower temperature in the pseudogap regime has been identified to have a d-form factor (15–18), and its temperature dependence (19–25) indicates that it is unlikely to be the origin of the pseudogap present at higher temperature. Similar considerations apply to other fluctuating order models (26) based on AF or d-wave superconductor.

We are therefore led to an alternative perspective (3), in which the pseudogap metal represents a new quantum state that could be stable down to very low T, at least for model Hamiltonians not too different from realistic cuprate models. The observed low-T DW order is then presumed to be an instability of the pseudogap metal (27–31). An early discussion (32) of the pseudogap metal proposed a state that was a doped spin liquid with "spinon" and "holon" excitations fractionalizing the spin and charge of an electron: the spinon carries spin $S = 1/2$ and is charge neutral, whereas the holon is spinless and carries charge $+e$. However, this state is incompatible with the sharp "Fermi arc" photoemission spectrum (7) around the diagonals of the Brillouin zone: the spin liquid has no sharp excitations with the quantum number of an electron and so will only produce broad multiparticle continua in photoemission.

Instead, we need a quantum state that has long-lived electron-like quasiparticles around a Fermi surface of size p, even though such a Fermi surface would violate the Luttinger relation of a Fermi liquid. The fractionalized Fermi liquid (FL*) (33) fulfills these requirements.

Significance

The most interesting states of the copper oxide compounds are not the superconductors with high critical temperatures. Instead, the novelty lies primarily in the higher temperature metallic "normal" states from which the superconductors descend. Here, we develop a simple, intuitive model for the physics of the metal at low carrier density, in the "pseudogap" regime. This model describes an exotic metal that is similar in many respects to simple metals like silver. However, the simple metallic character coexists with "topological order" and long-range quantum entanglement previously observed only in exotic insulators or fractional quantum Hall states in very high magnetic fields. Our model is compatible with many recent observations, and we discuss more definitive experimental tests.
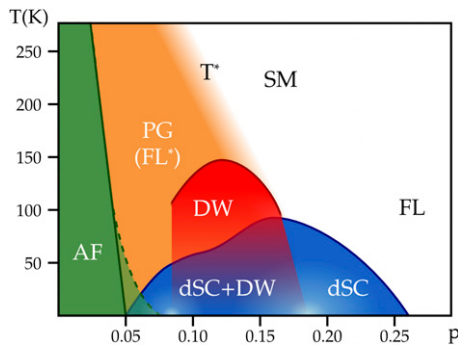
Fig. 1. Schematic phase diagram of hole-doped cuprates (apart from those with La doping) as a function of temperature (T) and hole density (p). The antiferromagnetic (AF) insulator is present near $p=0$, and the d-wave superconductor (dSC) is present below a critical temperature T_c. The pseudogap (PG) is present for $T < T^*$ and acquires density wave (DW) order at low T. The metallic states are the PG metal, the conventional Fermi liquid (FL), and the strange metal (SM). The dimer model of the present paper describes only the PG metal as a fractionalized Fermi liquid (FL*).

Fractionalized Fermi Liquids

The key to understanding the FL* state is the topological nature of the Luttinger relation for the area enclosed by the Fermi surface. For the case of a conventional FL state, Oshikawa (34) provided a nonperturbative proof of the Luttinger relation by placing the system on a torus, and computing the response to a single flux quantum threaded through one of the holes of the torus. His primary assumption about the many-body state was that its only low-energy excitations were fermionic quasiparticles around a Fermi surface. This assumption then points to a route to obtaining a Fermi surface of a different size (35): we need a metal that, in addition to the quasiparticle excitations around the Fermi surface, has global topological excitations nearly degenerate with the ground state, similar to those found in insulating spin liquids (36, 37). In the context of the doped spin liquids noted earlier, we obtain a FL* state when the holon and spinon bind to form a fermionic state with spin $S = 1/2$ and charge $+e$ (a possible origin of the binding is the attraction arising from the nearest-neighbor hopping), and there is a Fermi surface with quasiparticle excitations of this bound state (38–40) [other possibilities for the fate of this bound state have also been discussed (41)]. Such a Fermi surface has long-lived electron-like quasiparticles and encloses an area determined by density p, and not $1 + p$ (40, 42–44), just as required by observations in the pseudogap metal. Alternatively, a FL* phase can also be obtained from Kondo lattice models (45, 46), but we shall not use this here.

Earlier studies have examined a number of phenomenological and path integral models of FL* theories of the pseudogap (39, 40, 42–44) [and in an ansatz for the pseudogap (47)]. These models contain emergent gauge field excitations, which are needed to provide the global topological states required to violate the Luttinger relation of the FL state. However, they also include spurious auxiliary particle states that are only approximately projected out. The gauge field can undergo a crossover to confinement, but the present models do not keep close track of lattice-scale Berry phases that control the appearance of density wave order in the confining state (48). Here, we propose to overcome these difficulties by a new quantum dimer model that can realize a metallic state that is a FL*. This should open up studies of the photoemission spectrum, density wave instabilities, and crossovers to confinement at low T in the pseudogap metal.

Quantum Dimer Models

Quantum dimer models (49–51) have been powerful tools in uncovering the physics of spin liquid phases, and of their instabilities

to conventional confining phases (52–54). Dimer models of doped spin liquids have also been studied (49, 55, 56), but all of these involve doping the insulating models by monomers that carry charge $+e$, but no spin. Here, we introduce an alternative route to doping, in which the dopants are dimers, carrying both charge and spin.

The Hilbert space of our dimer model is spanned by the close-packing coverings of the square lattice with two species of dimers (Fig. 2), with an additional twofold spin degeneracy of the second species. It can be mapped by an appropriate similarity transform (49) to a truncation of the Hilbert space of the t-J model.

The first species of dimers are bosons, $D_{i\eta}$, which reside on the link connecting the square lattice site $i \equiv (i_x, i_y)$ to the site $i + \hat{\eta}$, where $\hat{\eta} = \hat{x} \equiv (1,0)$ or $\hat{y} \equiv (0,1)$. These are the same as the dimers in the Rokhsar–Kivelson (RK) model (49), to which our model reduces at zero doping. When connecting to the Hilbert space of the t-J model, each boson maps to a pair of electrons in a spin-singlet state:

$$D_{i\eta}^\dagger |0\rangle \Rightarrow \Upsilon_{i\eta} \left(c_{i\uparrow}^\dagger c_{i+\hat{\eta},\downarrow}^\dagger + c_{i+\hat{\eta},\uparrow}^\dagger c_{i\downarrow}^\dagger \right) |0\rangle \Big/ \sqrt{2}, \qquad [1]$$

where $c_{i\alpha}$ is the electron annihilation operator on Cu site i with spin $\alpha = \uparrow, \downarrow$, and $|0\rangle$ is the empty state with no dimers or electrons. The phase factors $\Upsilon_{i\eta}$ depend upon a gauge choice: for the choice made by RK, $\Upsilon_{iy} = 1$ and $\Upsilon_{ix} = (-1)^{i_y}$.

The second species of dimers are "fermions," $F_{i\eta\alpha}$ with $\alpha = \uparrow, \downarrow$, which carry spin $S = 1/2$ and charge $+e$ relative to the half-filled insulator, and are present with a density p. Each fermionic dimer maps to a bound state of a holon and a spinon, which we take to reside on a bonding orbital between nearest-neighbor sites:

$$F_{i\eta\alpha}^\dagger |0\rangle \Rightarrow \Upsilon_{i\eta} \left(c_{i\alpha}^\dagger + c_{i+\hat{\eta},\alpha}^\dagger \right) |0\rangle \Big/ \sqrt{2}. \qquad [2]$$

In a three-band model (57, 58), the state $F_{i\eta\alpha}^\dagger |0\rangle$ can be identified with the $S = 1/2$ state of a hole delocalized over a O site and its two Cu neighbors, considered by Emery and Reiter (59, 60).

Let us stress our assumption that spinon and holon bind not because of confinement but because of a short-range attraction. Therefore, the bound state (2) can break up at an energy cost of order the antiferromagnetic exchange, and the holon and spinon appear as gapped, free excitations that would contribute two-particle continuum spectra to photoemission or neutron scattering
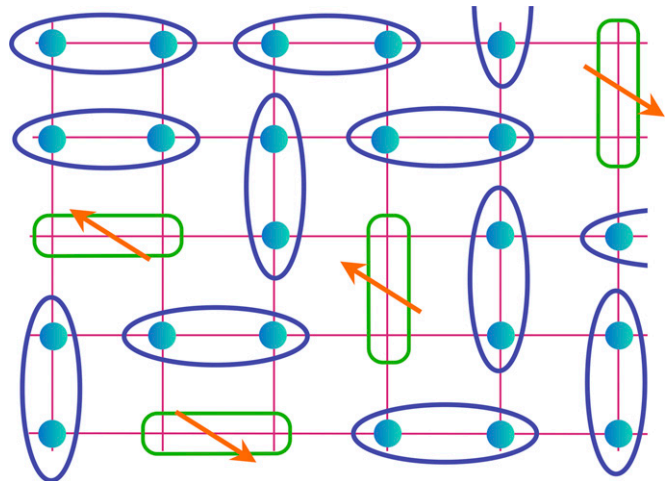
Fig. 2. A typical dimer configuration identifying a state in the Hilbert space. The blue ellipses are the bosons $D_{i\eta}$, which are spinless and neutral. The green rectangles are the fermions $F_{i\eta\alpha}$, which carry spin $S = 1/2$ and charge $+e$. The density of the $F_{i\eta\alpha}$ dimers is p.

spectra. These fractionalized states can be included in our dimer model by expanding the Hilbert space to include monomers, but we will not do so here because we focus on the lowest energy sector. As a consequence, there is no monomer Fermi surface (42) in the present model of the pseudogap metal.

The states 1 and 2 are precisely those that dominate in the two-site dynamical mean field theory (DMFT) analysis of the Hubbard model by Ferrero et al. (61): they correspond to the S and $1+$ states of ref. 61, respectively, which are shown in figure 15 of this study to be the dominant components of the ground-state wave function at small p (see also ref. 62). The DMFT analysis captures important aspects of pseudogap physics, but with a coarse momentum resolution of the Brillouin zone. In DMFT, the states on the two-site cluster interact with a self-consistent environment in a mean-field way: the equations have so far only been solved at moderate temperatures and the nature of the ultimate ground state at low doping remains unclear. Our dimer model is a route to going beyond DMFT, and to include the nontrivial entanglement between these states on different pairs of sites in a non-mean field manner. The local constraints between different pairs of dimers are accounted for, allowing for the emergence of gauge degrees of freedom.

The original RK model can be mapped to a compact U(1) lattice gauge theory (50, 52, 53). In the doped dimer models studied earlier, the monomers then carry U(1) gauge charges of ± 1 on the two sublattices. By the same reasoning, we see that the $F_{\eta\alpha}$ fermions carry no net gauge charge, but are instead dipoles under the U(1) field.

We can now describe our realization of the pseudogap metal. We envisage a state where the confinement length scale of the compact U(1) gauge field is large, and specifically, larger than the spacing between the $F_{\eta\alpha}$ fermions. Then the $F_{\eta\alpha}$ fermions can move coherently in the presence of a dipolar coupling to the gauge fluctuations (40), and they will form Fermi surfaces enclosing total area p, thus realizing a FL* state. The confinement scale becomes large near the solvable RK point in the RK model (63, 64), near a Higgs transition to a $\mathbb{Z}_2$ spin liquid induced by allowing for diagonal dimers (54, 65–67), or more generally near a deconfined critical point (39). Our approach yields a "minimal model" for realizing FL* (which can be a stable, deconfined state in the $\mathbb{Z}_2$ spin liquid case), and confinement transitions in metals.

We present results below for the following Hamiltonian, illustrated in Fig. 3, acting on the dimer Hilbert space described above:

$$H = H_{RK} + H_1 + H_2$$

$$H_{RK} = \sum_i \Big[-J\, D_{ix}^\dagger D_{i+\hat{y},x}^\dagger D_{iy} D_{i+\hat{x},y} + 1 \text{ term}$$

$$+ V\, D_{ix}^\dagger D_{i+\hat{y},x}^\dagger D_{ix} D_{i+\hat{y},x} + 1 \text{ term} \Big]$$

$$H_1 = \sum_i \Big[-t_1\, D_{ix}^\dagger F_{i+\hat{y},x\alpha}^\dagger F_{ix\alpha} D_{i+\hat{y},x} + 3 \text{ terms}$$

$$-t_2\, D_{i+\hat{x},y}^\dagger F_{iy\alpha}^\dagger F_{ix\alpha} D_{i+\hat{y},x} + 7 \text{ terms}$$

$$-t_3\, D_{i+\hat{x}+\hat{y},x}^\dagger F_{iy\alpha}^\dagger F_{i+\hat{x}+\hat{y},x\alpha} D_{iy} + 7 \text{ terms}$$

$$-t_3\, D_{i+2\hat{y},x}^\dagger F_{iy\alpha}^\dagger F_{i+2\hat{y},x\alpha} D_{iy} + 7 \text{ terms} \Big], \quad [3]$$

where the undisplayed terms are generated by operations of the square lattice point group on the terms above. The first term, H_{RK}, coincides with the RK model for the undoped dimer model at $p = 0$. Single fermion hopping terms are contained in H_1, with hoppings t_i, which are expected to be larger than J. A perturbative estimate of the dimer hopping amplitudes t_i in terms
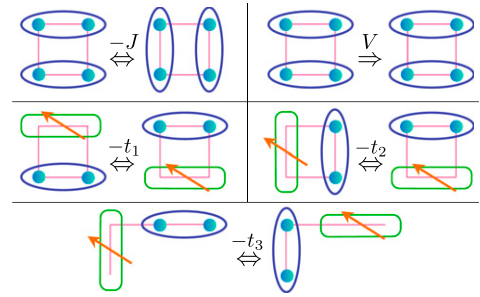
Fig. 3. Terms in the Hamiltonian $H_{RK} + H_1$.

of electron-hopping parameters can be found in *SI Appendix*. Note that all such terms must preserve the dimer close-packing constraint on every site, and we have chosen three terms with short-range hopping; longer-range hopping terms for the fermionic dimers are also possible, but expected to decay with distance, and are omitted for simplicity. Finally, H_2 allows for interactions between the fermionic dimers, with terms of the following form:

$$H_2 \sim \sum_i \Big(F_{ix\beta}^\dagger F_{i+\hat{y},x\alpha}^\dagger - F_{ix\alpha}^\dagger F_{i+\hat{y},x\beta}^\dagger \Big) F_{iy\beta} F_{i+\hat{x},y\alpha} + \dots, \quad [4]$$

which preserve the dimer constraint and spin rotation invariance. Purely fermionic dimer models with similar dimer hopping terms have been considered by Pollmann et al. (68).

Results

We now present results for the dispersion and quasiparticle residue of a single fermion described by $H_{RK} + H_1$; the interaction terms in H_2 play no role here. At a small p, the interactions between the fermionic dimers can be treated by a dilute gas expansion in p, whereas the dominant contributions to the quasiparticle dispersion and residue arise from the interaction between a single fermion and the close-packed sea of bosonic dimers. We computed the latter effects by exactly diagonalizing the singe fermion Hamiltonian on lattice sizes up to 8×8 with periodic boundary conditions, with the largest matrix of linear size 76,861,458. The RK model has two conserved winding numbers in a torus geometry, and these conservation laws also hold for our model: all results presented here are for the case of zero winding numbers. We extend these results to nonzero fermion density by interpolation in *SI Appendix*.

Our numerical study explored the dispersion of a single fermion over a range of values of the hopping parameters. We show in Fig. 4 the dispersion $\varepsilon(\mathbf{k})$ for a single $F_{\eta\alpha}$ fermion for hopping parameters obtained by a perturbative connection on a *t*-J model appropriate for the cuprates at the RK point $V = J = 1$. *SI Appendix* has similar results for additional parameter values.

The minima of the fermion dispersion were found at different points in the Brillouin zone, but there was a wide regime with minima near momenta $\mathbf{k} = (\pm\pi/2, \pm\pi/2)$. In fact, for the momentum points allowed on a 8×8 lattice, the global minimum of the dispersion in Fig. 4 is exactly at $(\pi/2, \pi/2)$. However, it is also clear from the figure that the dispersion is not symmetric about the antiferromagnetic Brillouin zone boundary, and that any interpolating function will actually have a minimum at (k_m, k_m) with $k_m < \pi/2$. A dispersion with these properties is of experimental interest because it will lead to formation of hole pockets near the minima for the dimer model with a nonzero density of $F_{\eta\alpha}$ fermions. Fig. 5 shows that changes to the dispersion from a 6×6 lattice are smaller than 5%.

Fig. 4. Lowest energy of a single-charge $+e\,F_{\eta\alpha}$ fermion as a function of momentum $\mathbf{k}$. We take hopping parameters obtained from the t-J model, $t_1 = -1.05$, $t_2 = 1.95$, and $t_3 = -0.6$, at the RK point $V = J = 1$ on a 8×8 lattice with periodic boundary conditions and zero winding numbers. Note that the dispersion is not symmetric about the magnetic Brillouin zone boundary, i.e., across the line connecting $(\pi, 0)$ to $(0, \pi)$. Line cuts of this dispersion are in Fig. 5.

Our numerical results also yield interesting information on the quasiparticle residue of the electron operator. This is nontrivial even for the case of a single fermionic dimer, because, unlike a free electron, a fermionic dimer can only move by "resonating" with the background of bosonic dimers, as is clear from Fig. 3. In the presence of a finite density of fermionic dimers, there will be an additional renormalization from the interaction between the fermions that we will not compute here. We do not expect this to have a significant $\mathbf{k}$ dependence around the hole pockets. In the dimer model subspace defined by the states in Eqs. **1** and **2**, the electron annihilation operator on site i has the same matrix elements as the following:

$$C_{i\alpha} = \frac{\epsilon_{\alpha\beta}}{2}\left(F^\dagger_{ix\beta}D_{ix} + F^\dagger_{i-\hat{x},x\beta}D_{i-\hat{x},x} + F^\dagger_{iy\beta}D_{iy} + F^\dagger_{i-\hat{y},y\beta}D_{i-\hat{y},y}\right), \quad [5]$$

relating the site to the four bonds around it ($\epsilon_{\alpha\beta}$ is the unit antisymmetric tensor). Then the quasiparticle residue is obtained by computing the following:

$$\mathcal{Z}(\mathbf{k}) = |\langle\Psi_F(\mathbf{k})|C_\alpha(-\mathbf{k})|\Psi_{RK}\rangle|^2, \quad [6]$$

where $|\Psi_{RK}\rangle$ is the ground state of the undoped model H_{RK}, and $|\Psi_F(\mathbf{k})\rangle$ is the ground state of $H_{RK} + H_1 + H_2$ in the sector with one $F_{\eta\alpha}$ fermion and total momentum $\mathbf{k}$ [the energy difference between these two states is $\varepsilon(\mathbf{k})$]. We show the values of $\mathcal{Z}(\mathbf{k})$ in Fig. 6, with parameters the same as those in Fig. 4. Note the strong suppression of the residue in the second antiferromagnetic Brillouin zone; line-cut plots of $\mathcal{Z}(\mathbf{k})$ in Fig. 5 highlight this suppression. We found this suppression of $\mathcal{Z}(\mathbf{k})$ to be a robust property in the regime of hopping parameters (with $t_2 > 0$) that had minima in the fermion dispersion along the Brillouin zone diagonal. This result implies that the quasiparticle residue will be highly anisotropic around the hole pockets that appear in the finite fermion density case, with little spectral weight along the "back side" of the pocket.

It is also possible to study the system in perturbation theory in t_i/J. We begin with the model with one fermion at $t_1 = t_2 = t_3 = 0$. The problem reduces to that of finding the ground state of H_{RK} in the presence of a stationary fermionic dimer: it is possible to

do this analytically at the solvable RK point $V = J$, as described in *SI Appendix*. The fermion hoppings at nonzero t_i is then computed perturbatively in a single-particle tight-binding model, with hopping matrix elements determined by overlaps of the wave functions with a stationary fermion. At the RK point, each matrix element reduces to the evaluation of a dimer correlation function in the classical problem of close-packed dimers on the square lattice (69). The computation of these matrix elements, and the resulting fermion dispersion, is described in *SI Appendix*. This perturbative dispersion is found to be in good agreement with our exact diagonalization results only for $|t_i/J| \lesssim 0.01$. This rather small upper limit is likely a consequence of the gaplessness of the RK point, so that higher order corrections involve noninteger powers of t_i/J.

Discussion

In this article, we develop a new class of doped dimer models featuring coherent electronic quasiparticle excitations on top of a spin-liquid ground state. The scenario considered here is based on the assumption that spinons and holons form bound states on nearest-neighbor sites. These fermionic bound states with spin $S = 1/2$ and charge $+e$ form a Fermi sea with density p and are observable as electronic quasiparticles in experiments. Such a Fermi sea realizes a topological quantum state called the "fractionalized Fermi liquid" (33), whose Fermi surfaces encloses

Fig. 5. Line cuts of the dispersion in Fig. 4 (*Top*) and of the quasiparticle residue in Fig. 6 (*Bottom*). Also shown are the results from exact diagonalization on a 6×6 lattice for comparison (red squares), which has a different set of allowed momentum points. The overall shape of the dispersion remains the same as for the 8×8 lattice, and the fractional changes to $\varepsilon(\mathbf{k})$ are smaller than 5%. The *Inset* shows the residue between $(0,0)$ and (π,π) on a logarithmic scale.

PHYSICS

Fig. 6. Quasiparticle residue of a charge $+e$ fermion computed from Eq. **6** for the parameters in Fig. 4, for a 8×8 lattice. The symmetry of the wave function yields $\mathcal{Z}(\mathbf{k}) = 0$ for all points between (π, π) and $(\pi, 0)$. Line cuts of $\mathcal{Z}(\mathbf{k})$ are in Fig. 5.

an area distinct from the Luttinger value in a conventional Fermi liquid.

The undoped RK model on the square lattice features a deconfined spin liquid ground state only at the special RK point $J = V$, whereas the ground state breaks lattice symmetries away from this point. Consequently, our numerical results of a single fermionic dimer coupled to the background of bosonic dimers focused at the RK point to uncover properties of the FL* state. At finite densities of fermionic dimers, we expect that our model (**3**) features a FL* phase in an extended parameter range. However, similar to the RK model, we also expect a wide parameter regime where our model has a ground state with broken lattice symmetries. We leave the computation of the phase diagram of our model for future study.

The main implication of our model of the pseudogap metal (in zero applied magnetic field and at moderate T below T^*) is that there are four well-formed pockets of charge $+e$ fermions carrying spin $S = 1/2$ in the vicinity of (but not exactly centered at) momentum $(\pi/2, \pi/2)$. The total area enclosed by these pockets is $2\pi^2 p$. Clearly, such pockets can immediately explain the Fermi liquid-like transport observed in recent optical (12) and

magnetoresistance (13) measurements. We also note that the hopping of electrons between CuO_2 layers requires to break either fermonic or bosonic dimers in our model, which naturally accounts for the observed gap in c-axis optical conductivity.

Experiments that involve removing one electron from the system (such as photoemission) have difficulty observing the back sides of the pockets because of the small (but nonzero) quasiparticle residue $\mathcal{Z}(\mathbf{k})$ noted above (Fig. 6). We propose this feature as an explanation for the photoemission observation of ref. 7 in the pseudogap metal. For further studies of these pockets, it would be useful to use experimental probes of the Fermi surface that keep the electrons within the sample (70): possibilities include ultrasound attenuation, optical Hall, and Friedel oscillations.

Our theory can be loosely summarized by "the electron becomes a dimer in the pseudogap metal," as in Eq. **5**: with a spin-liquid background present, there can be no single-site state representing an electron, and a dimer is the simplest possibility.

The main advantage of our quantum dimer model over previous treatments (39, 40, 42–44) of fractionalized Fermi liquids (FL*) is that it properly captures lattice-scale dispersions, quasiparticle residues, and Berry phases: all of these are expected to play crucial roles in the crossovers to confinement and associated symmetry breaking at low T (48, 52, 53). Given the elongated dimer and dipolar nature of the electron, Ising-nematic order (71) is a likely possibility; the d-form factor density wave (15, 16) is then a plausible instability of such a nematic metal. The interplay between the monopole-induced crossovers to confinement (52, 53) and the density wave instabilities of the hole pockets (30, 31) can also be examined in such dimer models. The onset of superconductivity will likely require additional states, such as a spinless, charge $+2e$ boson consisting of a pair of empty sites.

1. Bhattacharya S, et al. (1988) Anomalous ultrasound propagation in the high-T_c superconductors: $La_{1.8}Sr_{0.2}CuO_{4-y}$ and $YBa_2Cu_3O_{7-\delta}$. *Phys Rev B Condens Matter* 37(10): 5901–5904.
2. Alloul H, Mendels P, Collin G, Monod P (1988) ^{89}Y NMR study of the Pauli susceptibility of the CuO_2 planes in YBa_2Cu. *Phys Rev Lett* 61(6):746–749.
3. Chowdhury D, Sachdev S (2015) The enigma of the pseudogap phase of the cuprate superconductors. arXiv:1501.00002.
4. Platé M, et al. (2005) Fermi surface and quasiparticle excitations of overdoped $Tl_2Ba_2CuO_{6+\delta}$. *Phys Rev Lett* 95(7):077001.
5. Damascelli A, Hussain Z, Shen Z-X (2003) Angle-resolved photoemission studies of the cuprate superconductors. *Rev Mod Phys* 75:473–541.
6. Shen KM, et al. (2005) Nodal quasiparticles and antinodal charge ordering in $Ca_{2-x}Na_xCuO_2Cl_2$. *Science* 307(5711):901–904.
7. Yang H-B, et al. (2011) Reconstructed Fermi surface of underdoped $Bi_2Sr_2CaCu_2O_{8+\delta}$ cuprate superconductors. *Phys Rev Lett* 107(4):047003.
8. Ando Y, Kurita Y, Komiya S, Ono S, Segawa K (2004) Evolution of the Hall coefficient and the peculiar electronic structure of the cuprate superconductors. *Phys Rev Lett* 92(19):197001.
9. Orenstein J, et al. (1990) Frequency- and temperature-dependent conductivity in $YBa_2Cu_3O_{6+x}$ crystals. *Phys Rev B Condens Matter* 42(10):6342–6362.
10. Uchida S, et al. (1991) Optical spectra of $La_{2-x}Sr_xCuO_4$: Effect of carrier doping on the electronic structure of the CuO_2 plane. *Phys Rev B Condens Matter* 43(10):7942–7954.
11. Lee PA, Nagaosa N, Wen X-G (2006) Doping a Mott insulator: Physics of high-temperature superconductivity. *Rev Mod Phys* 78:17–85.

12. Mirzaei SI, et al. (2013) Spectroscopic evidence for Fermi liquid-like energy and temperature dependence of the relaxation rate in the pseudogap phase of the cuprates. *Proc Natl Acad Sci USA* 110(15):5774–5778.
13. Chan MK, et al. (2014) In-plane magnetoresistance obeys Kohler's rule in the pseudogap phase of cuprate superconductors. *Phys Rev Lett* 113(17):177005.
14. Allais A, Chowdhury D, Sachdev S (2014) Connecting high-field quantum oscillations to zero-field electron spectral functions in the underdoped cuprates. *Nat Commun* 5:5771.
15. Sachdev S, La Placa R (2013) Bond order in two-dimensional metals with antiferromagnetic exchange interactions. *Phys Rev Lett* 111(2):027202.
16. Fujita K, et al. (2014) Direct phase-sensitive identification of a d-form factor density wave in underdoped cuprates. *Proc Natl Acad Sci USA* 111(30):E3026–E3032.
17. Comin R, et al. (2015) Symmetry of charge order in cuprates. *Nat Mater*, 10.1038/nmat4295.
18. Forgan EM, et al. (2015) The nature of the charge density waves in under-doped $YBa_2Cu_3O_{6.54}$ revealed by X-ray measurements of the ionic displacements. arXiv: 1504.01585.
19. Wu T, et al. (2011) Magnetic-field-induced charge-stripe order in the high-temperature superconductor $YBa_2Cu_3O_y$. *Nature* 477(7363):191–194.
20. Wu T, et al. (2013) Emergence of charge order from the vortex state of a high-temperature superconductor. *Nat Commun* 4:2113.
21. Ghiringhelli G, et al. (2012) Long-range incommensurate charge fluctuations in $(Y,Nd)Ba_2Cu_3O_{6+x}$. *Science* 337(6096):821–825.
22. Achkar AJ, et al. (2012) Distinct charge orders in the planes and chains of ortho-III-ordered $YBa_2Cu_3O_{6+\delta}$ superconductors identified by resonant elastic x-ray scattering. *Phys Rev Lett* 109(16):167001.

23. Chang J, et al. (2012) Direct observation of competition between superconductivity and charge density wave order in $YBa_2Cu_3O_{6.67}$. *Nat Phys* 8(12):871–876.

24. LeBoeuf D, et al. (2013) Thermodynamic phase diagram of static charge order in underdoped $YBa_2Cu_3O_y$. *Nat Phys* 9(2):79–83.

25. Wu T, et al. (2015) Incipient charge order observed by NMR in the normal state of $YBa_2Cu_3O_y$. *Nat Commun* 6:6438.

26. Kivelson SA, et al. (2003) How to detect fluctuating stripes in the high-temperature superconductors. *Rev Mod Phys* 75:1201–1241.

27. Vojta M (2012) Stripes and electronic quasiparticles in the pseudogap state of cuprate superconductors. *Physica C Supercond* 481:178–188.

28. Comin R, et al. (2014) Charge order driven by Fermi-arc instability in $Bi_2Sr_{2-x}La_xCuO_{6+\delta}$. *Science* 343(6169):390–392.

29. da Silva Neto EH, et al. (2014) Ubiquitous interplay between charge ordering and high-temperature superconductivity in cuprates. *Science* 343(6169):393–396.

30. Chowdhury D, Sachdev S (2014) Density-wave instabilities of fractionalized Fermi liquids. *Phys Rev B* 90:245136.

31. Zhang L, Mei J-W (2014) Charge order instability in doped resonating valence bond state and magnetic orbits from reconstructed Fermi surface in underdoped cuprates: A phenomenological synthesis. arXiv:1408.6592.

32. Kotliar G, Liu J (1988) Superexchange mechanism and d-wave superconductivity. *Phys Rev B Condens Matter* 38(7):5142–5145.

33. Senthil T, Sachdev S, Vojta M (2003) Fractionalized fermi liquids. *Phys Rev Lett* 90(21): 216403.

34. Oshikawa M (2000) Topological approach to Luttinger's theorem and the Fermi surface of a Kondo lattice. *Phys Rev Lett* 84(15):3370–3373.

35. Senthil T, Vojta M, Sachdev S (2004) Weak magnetism and non-Fermi liquids near heavy-fermion critical points. *Phys Rev B* 69:035111.

36. Read N, Sachdev S (1991) Large-N expansion for frustrated quantum antiferromagnets. *Phys Rev Lett* 66(13):1773–1776.

37. Wen XG (1991) Mean-field theory of spin-liquid states with finite energy gap and topological orders. *Phys Rev B Condens Matter* 44(6):2664–2672.

38. Wen X-G, Lee PA (1996) Theory of underdoped cuprates. *Phys Rev Lett* 76(3):503–506.

39. Kaul R, Kolezhuk A, Levin M, Sachdev S, Senthil T (2007) Hole dynamics in an antiferromagnet across a deconfined quantum critical point. *Phys Rev B* 75:235122.

40. Qi Y, Sachdev S (2010) Effective theory of Fermi pockets in fluctuating antiferromagnets. *Phys Rev B* 81:115129.

41. Baskaran G (2007) 3/2-Fermi liquid: The secret of high-T_c cuprates. arXiv:0709.0902.

42. Kaul RK, Kim YB, Sachdev S, Senthil T (2008) Algebraic charge liquids. *Nat Phys* 4(1): 28–31.

43. Mei J-W, Kawasaki S, Zheng G-Q, Weng Z-Y, Wen X-G (2012) Luttinger-volume violating Fermi liquid in the pseudogap phase of the cuprate superconductors. *Phys Rev B* 85:134519.

44. Punk M, Sachdev S (2012) Fermi surface reconstruction in hole-doped *t-J* models without long-range antiferromagnetic order. *Phys Rev B* 85:195123.

45. Andrei N, Coleman P (1989) Cooper instability in the presence of a spin liquid. *Phys Rev Lett* 62(5):595–598.

46. Burdin S, Grempel DR, Georges A (2002) Heavy-fermion and spin-liquid behavior in a Kondo lattice with magnetic frustration. *Phys Rev B* 66:045111.

47. Yang K-Y, Rice TM, Zhang F-C (2006) Phenomenological theory of the pseudogap state. *Phys Rev B* 73:174501.

48. Read N, Sachdev S (1989) Valence-bond and spin-Peierls ground states of low-dimensional quantum antiferromagnets. *Phys Rev Lett* 62(14):1694–1697.

49. Rokhsar DS, Kivelson SA (1988) Superconductivity and the quantum hard-core dimer gas. *Phys Rev Lett* 61(20):2376–2379.

50. Fradkin E, Kivelson SA (1990) Short range resonating valence bond theories and superconductivity. *Mod Phys Lett B* 4(3):225–232.

51. Read N, Sachdev S (1989) Some features of the phase diagram of the square lattice SU(*N*) antiferromagnet. *Nucl Phys B* 316(3):609–640.

52. Read N, Sachdev S (1990) Spin-Peierls, valence-bond solid, and Néel ground states of low-dimensional quantum antiferromagnets. *Phys Rev B Condens Matter* 42(7): 4568–4589.

53. Sachdev S, Vojta M (1999) Translational symmetry breaking in two-dimensional antiferromagnets and superconductors. *J Phys Soc Jpn* 69(Suppl B):1.

54. Moessner R, Sondhi SL (2001) Resonating valence bond phase in the triangular lattice quantum dimer model. *Phys Rev Lett* 86(9):1881–1884.

55. Poilblanc D (2008) Properties of holons in the quantum dimer model. *Phys Rev Lett* 100(15):157206.

56. Lamas CA, Ralko A, Cabra DC, Poilblanc D, Pujol P (2012) Statistical transmutation in doped quantum dimer models. *Phys Rev Lett* 109(1):016403.

57. Emery VJ (1987) Theory of high-T_c superconductivity in oxides. *Phys Rev Lett* 58(26): 2794–2797.

58. Ebrahimnejad H, Sawatzky GA, Berciu M (2014) The dynamics of a doped hole in a cuprate is not controlled by spin fluctuations. *Nat Phys* 10(12):951–955.

59. Emery VJ, Reiter G (1988) Quasiparticles in the copper-oxygen planes of high-T_c superconductors: An exact solution for a ferromagnetic background. *Phys Rev B Condens Matter* 38(16):11938–11941.

60. Emery VJ, Reiter G (1990) Reply to "Validity of the *t-J* model." *Phys Rev B Condens Matter* 41(10):7247–7249.

61. Ferrero M, et al. (2009) Pseudogap opening and formation of Fermi arcs as an orbital-selective Mott transition in momentum space. *Phys Rev B* 80:064501.

62. Sordi G, Haule K, Tremblay A-MS (2011) Mott physics and first-order transition between two metals in the normal-state phase diagram of the two-dimensional Hubbard model. *Phys Rev B* 84:075161.

63. Vishwanath A, Balents L, Senthil T (2004) Quantum criticality and deconfinement in phase transitions between valence bond solids. *Phys Rev B* 69:224416.

64. Fradkin E, Huse DA, Moessner R, Oganesyan V, Sondhi SL (2004) Bipartite Rokhsar-Kivelson points and Cantor deconfinement. *Phys Rev B* 69:224415.

65. Sachdev S, Read N (1991) Large *N* expansion for frustrated and doped quantum antiferromagnets. *Int J Mod Phys B* 5:219–249.

66. Sachdev S (1992) Kagomé- and triangular-lattice Heisenberg antiferromagnets: Ordering from quantum fluctuations and quantum-disordered ground states with unconfined bosonic spinons. *Phys Rev B Condens Matter* 45(21):12377–12396.

67. Yao H, Kivelson SA (2012) Exact spin liquid ground states of the quantum dimer model on the square and honeycomb lattices. *Phys Rev Lett* 108(24):247206.

68. Pollmann F, Betouras JJ, Shtengel K, Fulde P (2011) Fermionic quantum dimer and fully-packed loop models on the square lattice. *Phys Rev B* 83:155117.

69. Samuel S (1980) The use of anticommuting variable integrals in statistical mechanics. I. The computation of partition functions. *J Math Phys* 21(12):2806–2814.

70. Chowdhury D, Sachdev S (2015) Higgs criticality in a two-dimensional metal. *Phys Rev B* 91:115123.

71. Kivelson SA, Fradkin E, Emery VJ (1998) Electronic liquid-crystal phases of a doped Mott insulator. *Nature* 393(6685):550–553.

PHYSICS